

WATER MIST SPRAY MODELLING WITH FDS

Simo Hostikka, Jukka Vaari, Topi Sikanen, Antti Paajanen

VTT Technical Research Centre of Finland
P.O.Box 1000, Espoo
FI-02044 VTT, Finland
e-mail: simo.hostikka@vtt.fi

ABSTRACT

Numerical simulation of water mist systems is gaining interest among fire safety engineers due to the increasing range of water mist suppression and protection applications, and the lack of simple and general design rules. The existing Eulerian-Lagrangian framework of FDS can be used for water mist simulations, but the published reports on the simulation process and validations are few. In comparison to traditional sprinkler technology, water mist has a wider range of physical suppression and cooling effects. An accurate modeling of such systems requires that all the relevant input parameters can be prescribed. From the modeling viewpoint, an important difference is the stronger exchange of momentum between the gas and liquid phases. The FDS capabilities and improvements concerning the spray dynamics and heat transfer, including the experimental validation, are presented. The experimental work includes the measurements of drop size, drop speed and mist flux profiles, gas phase entrainment speed in a channel geometry and radiative heat flux attenuation.

INTRODUCTION

Over the past 20 years, demonstrating the suppression performance of fixed water-based fire fighting systems has been done through full-scale fire testing, although tentative computational capabilities and tools for predicting the suppression system performance have existed all along. Water mist systems represent a recent development for water based fire suppression technology. The 20-year commercial history of water mist systems has seen a large number of experiments, but no general design and installation rules have emerged. This is primarily because there are several extinguishing mechanisms for water mist, the most important being gas-phase cooling, surface wetting, and scattering and absorption of heat radiation. The relative importance of the mechanisms is difficult to quantify as it depends on the technical details of the water mist system, as well as the application.

The R&D of large fire suppression systems calls for abundant resources both in terms of time and money. It can be expected that the need for full scale

experiments can be reduced by making use of state-of-the-art fire simulation software in the R&D process. Such tools are in everyday use in the field of Fire Safety Engineering. Yet, these tools have not been applied in simulating the performance of active fire suppression systems. This development is seen as evident in the near future, and indeed it is recently recognized as the top priority by the International Forum of Fire Research Directors (Grosshandler 2007).

In this presentation, we present enhancements to and validation of Fire Dynamics Simulator (FDS) (McGrattan et al. 2007) in describing water spray dynamics, air entrainment and radiation attenuation.

SPRAY COMPUTATIONS IN FDS

The motion of a single spherical droplet is governed by the equation of motion, considering acceleration by gravity and drag between the gas and a droplet.

$$\frac{dm_d \mathbf{u}}{dt} = m_d \mathbf{g} - \frac{1}{2} \rho_g C_D \pi r_d^2 \|\mathbf{u}_{rel}\| \mathbf{u}_{rel} \quad (1)$$

where m_d is the droplet mass, \mathbf{u} is the droplet velocity, \mathbf{g} is the gravity vector, C_D is the drag coefficient, r_d is the droplet radius and \mathbf{u}_{rel} is the relative velocity between droplet and gas. Recently, Randall McDermott and Howard Baum of NIST have developed an analytical solution for the droplet and gas velocities in a multi-droplet-gas system during a short time interval. This analytical solution is used to update the droplet positions and velocities, as well as gas velocity, during each FDS time step.

In dense sprays, the individual droplets can start to influence each other through aerodynamic interactions. These aerodynamic interactions become important when the average droplet spacing is less than 10 droplet diameters. This corresponds approximately to a droplet volume fraction $\alpha = 0.01$, achievable in some water mist suppression systems. The reduction of hydrodynamic forces to the second (trailing) sphere due to the wake effect is calculated using the correlation developed by Ramírez-Munoz et al. (2007). The drag coefficient is calculated as $C_D = (F/F_0) C_{D0}$, where C_{D0} is the drag coefficient of a single droplet. The ratio of hydrodynamic forces on trailing and single droplets is

$$\frac{F}{F_0} = W \left[1 + \frac{\text{Re}_1}{16} \frac{1}{(L/d_d - \frac{1}{2})^2} \exp\left(-\frac{\text{Re}_1}{16} \frac{1}{(L/d_d - \frac{1}{2})}\right) \right], \quad (2)$$

where Re_1 is the single droplet-Reynolds number, L is the distance between the droplets and W is the non-dimensional, non-disturbed wake velocity at the centre of the trailing droplet

$$W = 1 - \frac{C_{D0}}{2} \left[1 - \exp\left(-\frac{\text{Re}_1}{16} \frac{1}{(L/d_d - \frac{1}{2})}\right) \right]. \quad (3)$$

In above, d_d is the droplet radius. This model assumes that the trailing droplets are perfectly in line, and thus provides an upper bound estimate for the drag reduction. On the other hand, a comparison against the results by Prah et al. (2009) suggests that the above correlation underestimates the drag reduction when $L/d_d < 3$.

Droplets are introduced in to the computational domain on a segment of a spherical surface with origin at the sprinkler nozzle location and radius determined by the offset parameter. The spray angle outlines the solid angle of this sphere segment. The insertion points of the particles are selected as follows. The longitude θ is uniformly distributed between 0 and 2π . The latitude is randomly chosen from a probability density function

$$P_\phi = f(\phi) \sin \phi \quad (4)$$

where $f(\phi)$ is a distribution function. In the following simulations, a Gaussian profile was assumed

$$f(\phi) = \exp\left[-\beta(\mu - x)^2\right], \quad x = \frac{\phi_{\max} - \phi}{\phi_{\max} - \phi_{\min}} \quad (5)$$

Here ϕ_{\min} and ϕ_{\max} are the angles that outline the spray cone. For full cone sprays, the default parameters are $\beta = 5$ and $\mu = 0$.

The cumulative volume fraction of droplet diameters follows a distribution that is a combination of lognormal and Rosin-Rammler distributions:

$$F(d) = \begin{cases} \frac{1}{\sqrt{2\pi}} \int_0^d \frac{1}{\sigma d'} e^{-\frac{[\ln(d'/d_m)]^2}{2\sigma^2}} dd' & d \leq d_m \\ 1 - e^{-0.693\left(\frac{d}{d_m}\right)^\gamma} & d_m < d \end{cases} \quad (6)$$

By default $\sigma = 1.15/\gamma$ so that the probability density function is continuous. In simulations the particle size is bounded from below. Smaller droplets are assumed to vaporize instantly. The median droplet

size depends on the operating pressure used. Since the experimental droplet size distribution is determined at certain pressure, this variation in droplet size is taken into account by scaling the median droplet size as $d_m \propto p^{-1/3}$.

The spray dynamics involves strong coupling between the Lagrangian and Eulerian phases. For the simulation of the water mist sprays, the accuracy of spray turbulence is very important. The inclusion of dynamic sub-grid scale turbulence model in FDS6 provided a significant improvement in the spray predictions of the spray width and velocities.

The main features of the radiation-spray interaction model are described in Hostikka & McGrattan 2006. The most important difference between the current model and the original version described in the references is the use of single droplet diameter for the spray radiation property calculation instead of averaging over the drop size distribution. During the simulation, the properties are found from a look-up table using the local Sauter-mean diameter d_{32} . This method is expected to be better justified in situations where the local drop size distribution has not the same functional form as the original size distribution.

EXAMPLE NOZZLES

The example nozzles were Spraying Systems LN-2 and three high pressure micro nozzles A, B and C from Marioff Corporation. They were modelled using the knowledge of the operating pressures, experimentally determined flow rates and droplet size distributions. The droplets were introduced to the simulation domain on a section of a spherical surface 0.05...0.1 meters away from the nozzle location.

The spray angles were determined from close-up photographs. The initial droplet velocities were calculated from the pipe pressure ΔP

$$v_{d,0} = C \sqrt{\frac{2\Delta P}{\rho_d}} \quad (7)$$

where ρ_d is water density and C was taken to be 0.95 to account for friction. The droplet size distribution parameters were found by least squares fit of Eq. (6) to the experimentally determined cumulative volume distribution. Fitting the FDS cumulative number distribution to the experimentally measured cumulative number distribution was also tested and it was discovered that these two methods resulted in significantly different distribution parameters. For nozzle C, this method was used. An example of size distribution is shown in Figure 1 for nozzle A. The model parameters are listed in Table 1.

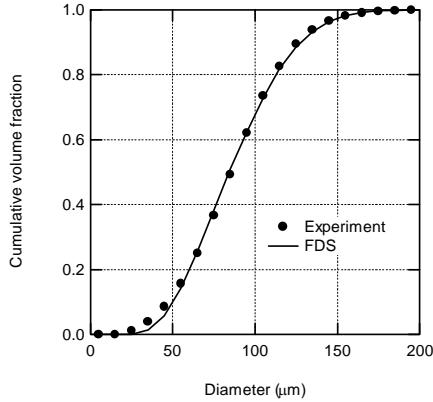


Figure 1: FDS droplet size distribution fitted to the experimental data for nozzle A.

Table 1: Model parameters for nozzles.

nozzle	K (l/min/bar ^{1/2})	ϕ (deg)	d_m (μm)	γ	σ
LN-2	0.347	38	72	2.1	
A	0.2	10	83	2.9	0.4
B	0.433	12	79	2.26	0.5
C	0.767	14	102	2.59	0.52

The multi-orifice spray heads used in this study are summarized in Table 2. They are constructed by attaching single orifice nozzles of types A, B and C into a spray head body. The assembled spray head has a centre nozzle spraying in the axial direction, and a number of orifices distributed evenly at the perimeter, each spraying at an angle with respect to the axial direction. In the simulations the multi-orifice spray heads were modeled using several individual single orifice nozzles placed at the same location with but with different orientations.

Table 2: The multi-orifice spray heads.

	SH1	SH2	SH3	SH4	SH5
Centre nozzle	A	C	B	B	B
Perimeter nozzle	A	B	A	B	B
Number of perimeter nozzles	6	6	8	8	8
Perimeter angle (deg)	60	60	45	45	30

RESULTS AND DISCUSSION

Spray profiles

Radial profiles of the mean droplet speed, mist flux and mean drop size were measured using direct imaging (DI) technique. In the simulations, the spray

profiles were determined with a simulated phase Doppler particle analyzer collecting droplet statistics from a 2-cm spherical volume around each measurement location.

A comparison between measured and simulated LN-2 profiles at distance 40 cm below the nozzle is shown in Figure 2. Pressure was 20 bar. Simulation results are computed at 1, 2 and 4 cm spatial resolutions. The simulated droplet speed profiles are not fully converged even at 1 cm resolution, as a mesh refinement tends to make the profile wider, reducing the peak value. The mist flux and mean diameter profiles are quite well converged, showing a reasonable agreement with experimental data. The experimental mist flux at spray axis is lower than at 5 cm distance, indicating that the assumption about full-cone profile with Gaussian distribution may not be correct.

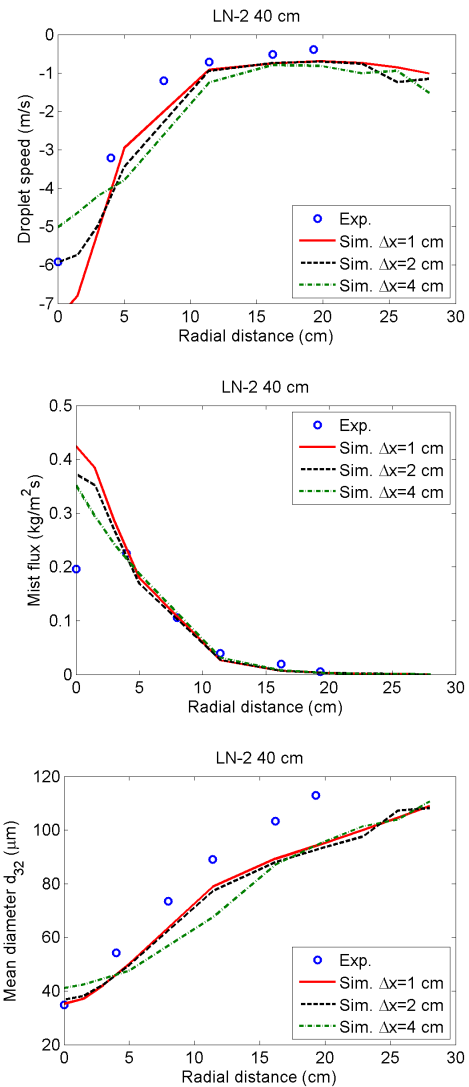


Figure 2: Experimental and simulated droplet speed, mist flux and mean diameter profiles for LN-2 nozzle.

It is interesting that the simulations can accurately predict the formation of the V-shaped diameter profile, caused by relatively higher proportion of large, high momentum droplets on the outer parts of the spray and accumulation of smaller droplets to the central spray by the air entrainment. Similar profile was also observed at a distance of 62 cm.

The experimental and simulated results for micro nozzles A, B and C at 70 bar pressure are shown in Figure 3. The experimental uncertainty of the results is high because sprays were sometimes un-symmetrical. The simulations were performed with 2-cm spatial resolution. Velocities show a reasonable agreement with experimental results. Mist fluxes on the spray centreline are significantly higher than the experimentally determined values. Further away from the spray centreline the discrepancy between the simulation and experiment diminishes. It should be noted however that there is considerable measurement uncertainty associated with the experimental mist flux values. Qualitatively the mist flux profiles are correct: there is a relatively thin dense core with a less dense outer spray as observed during experiments. The radial drop size profiles are found to be flat and quite different from the V-shaped profile observed for LN-2 nozzle. This may be due to the significantly higher initial speeds (112 m/s vs. 60 m/s) and the resulting difference in spray turbulence. The grid sensitivity study for nozzles A, B and C indicated that the 1 and 2 cm resolutions gave practically same results but 4 cm resolution showed significant differences. The results were not sensitive to the offset distance that was varied between 5 and 15 cm, but the velocity and mist flux profiles were very sensitive to 50 % variations in spray angle. In most simulations, 10^5 droplets per second per nozzle were introduced into computation. Increasing the number of particles to 10^6 or 10^7 per second tended to yield larger velocities on the spray centreline but did not otherwise affect the results.

The minimum diameter d_{\min} was set to $1 \mu\text{m}$ in most simulations. Sensitivity analysis showed that this parameter did not have a noticeable effect on the results. Restricting the global time-step or increasing the number of sub-time step iterations did not improve the results either.

The effect of aerodynamic interactions on water mist properties was investigated by running the simulations with the aerodynamic interaction model turned on and off. The drag reduction by aerodynamic interactions had a very modest effect on the results. The most noticeable effect was the slight flattening of the droplet diameter profile. The droplet volume fractions in the densest parts of the spray are just slightly over 0.01 for all nozzles. These results indicate that the inclusion of droplet-droplet aerodynamic interactions is not necessary for the

simulation of practical water mist systems. However, added cost of the drag reduction computation is small.

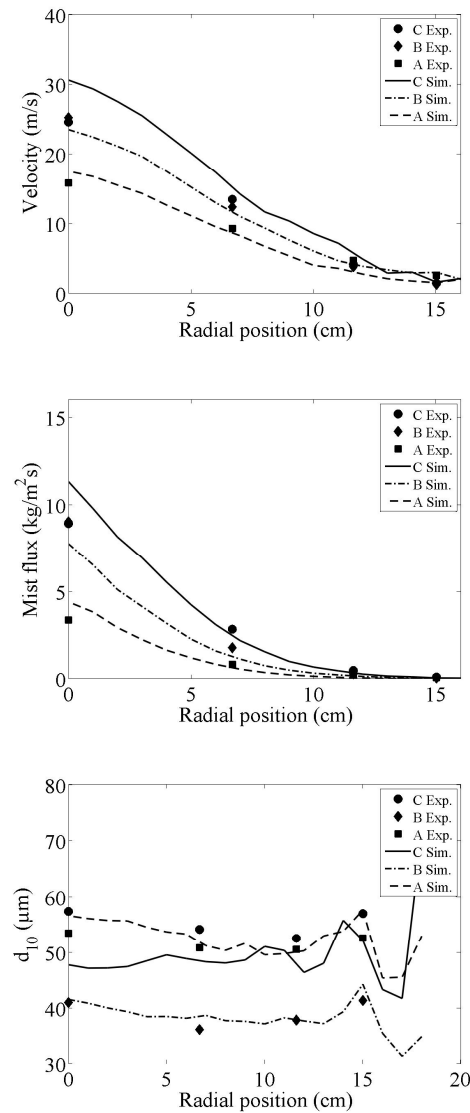


Figure 3: Experimental and simulated droplet speed, mist flux and mean diameter profiles of A, B and C micro nozzles.

Air entrainment

The capability of the water mist spray head to transfer the water momentum into the gas phase and to retain the entrained air flow is one of the main characteristics that determine how well the spray can penetrate into hot plumes and how efficiently the system can mix up the gas in closed space applications.

Air entrainment to the multi-orifice spray head water sprays was measured using a 2.0 m long a rectangular plywood channel having a cross section of 0.6 m by

0.6 m. A picture of the channel with a nozzle operating is shown in Figure 4. The spray heads were installed at the midpoint of the channel and they were spraying along the channel axis. The air velocity in the direction of the channel axis was measured with a bi-directional probe. Measurements were taken 0.5 m behind the nozzle on the channel axis and 0.06 m from the channel wall. The bi-directional probe and the associated differential pressure transducer were calibrated using a hot-wire anemometer. In each test, the water pressure was measured immediately outside the channel wall using a capacitive pressure transducer.

In the experiments, a wooden obstacle was placed close to the channel inlet, disturbing the entrainment airflow. To capture this effect, the computational domain was extended outside the channel. An overview of the simulation geometry is shown in Figure 4 (b). The spatial resolution in the simulations was 2 cm.

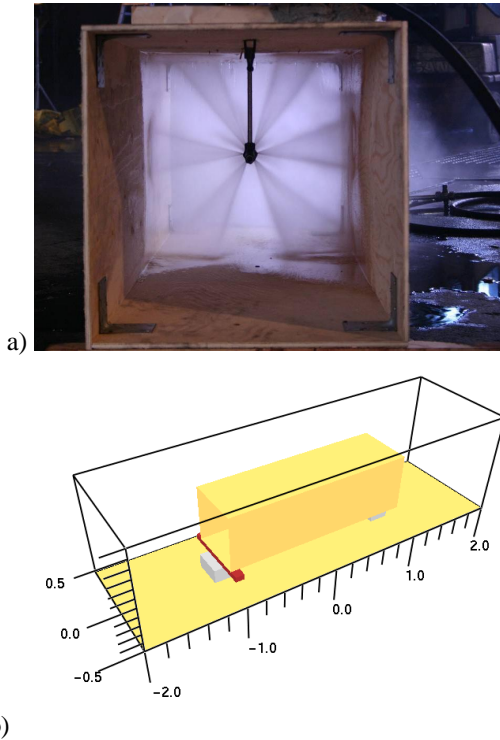


Figure 4: Air entrainment measurement channel picture (a) and FDS model (b).

Comparisons of the center line and close-to-the-wall velocities for the multi-orifice spray-heads are shown in Figures 5 (a) and (b), respectively. The agreement with experiment is good on the center line of the channel. While the spray heads SH4 and SH5 are both constructed from the same B type orifices, the velocities on the channel axis are slightly over predicted for SH4 and significantly under predicted for SH5. The difference between these spray heads is

in the amount of momentum injected in to the simulation. The SH5 spray-head has the perimeter nozzles at 30 degree angle, giving the highest momentum of all the spray heads considered in this paper. In general, we can conclude that the model is able to capture the effects of the pipe pressure and the main characteristic differences between the spray heads in terms of the air entrainment.

The offset parameter had a significant effect on the simulation results. Offset value of 4 cm was used here instead of the 10 cm. When using a smaller offset value, a reverse flow on the channel axis behind the spray head was observed. Appropriate offset value was found to depend on the numerical resolution used: The offset should be large enough to distribute the droplets within more than one computational cell. In the case of multi-orifice spray heads, it is also important to ensure that the grid is fine enough to resolve each of the spray jets. This may become a problem with small perimeter angles.

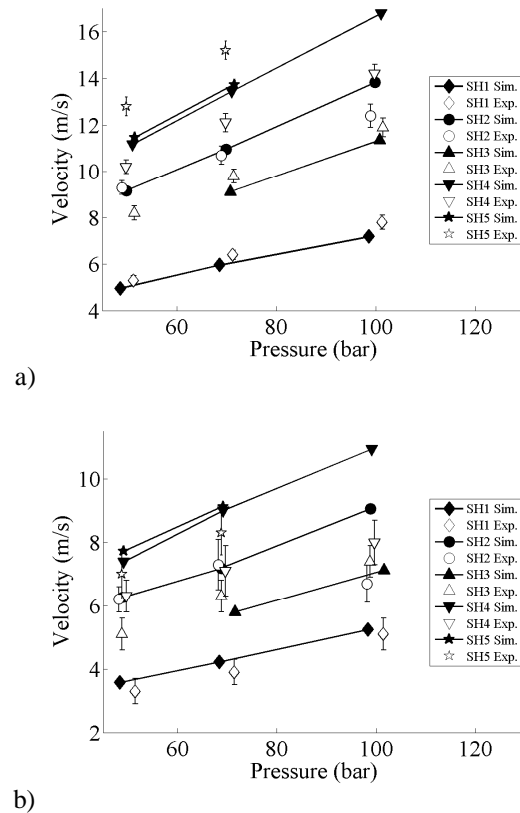


Figure 5: Air entrainment velocity for multi-orifice spray heads in (a) channel center and (b) 6 cm from the wall of the channel.

Radiation attenuation

The attenuation of thermal radiation by the micro nozzles A, B and C was measured using a radiant panel heat source and heat flux gauge. A schematic diagram of the experimental arrangement is shown in

Figure 6. The heat source was a LPG gas heater unit with a total heat output of 3.25 kW, radiating area of 20 cm x 30 cm and maximum surface temperature of 950 °C. The experiments were performed at 50, 70 and 100 bar pressures. The experimental uncertainty of the attenuation measurements was less than 7 % for nozzles A and B, and less than 2 % for nozzle C.

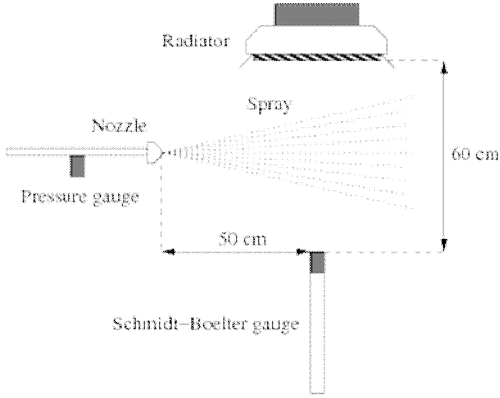


Figure 6: Experimental arrangement for the measurement of radiation attenuation.

The simulations were performed using two different sets of numerical parameters, listed in Table 3. For radiation related input parameters, the number of Mie-angles was set to 30 and the radiation source temperature to 950 °C. From the viewpoint of typical engineering applications, both parameter sets represent very well resolved simulations. For example, the spatial resolutions of 1.0...2.0 cm are seldom possible in full scale fire engineering applications. The better-than-usual resolutions are necessary due to the special characteristics of the validation simulation. To evaluate the predictive capability of the radiation model it is necessary to ensure that the numerical aspects of the solution do not dominate the errors.

Table 3: Numerical parameters in the radiation attenuation simulations.

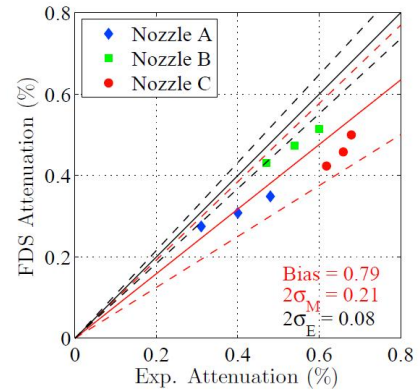
Numerical parameter	Set 1	Set 2
Spatial resolution (Δx)	2.0 cm	1.0 cm
Angular resolution N_Ω	1000	5000
Droplet insertion rate	1×10^5 1/s	1×10^6 1/s
Droplet CFL-condition	∞	1.0

The high angular resolution is necessary because the heat source represents only about 1 % of the full 4π solid angle for the point observer at 0.6 m distance. Using the default angular resolution of 100 angles would mean that the whole source would be represented by practically one control angle, i.e. one discrete intensity solution. Using the 1000 angles means that at least 10 angles can contribute to the radiation at the measurement location. Naturally, this

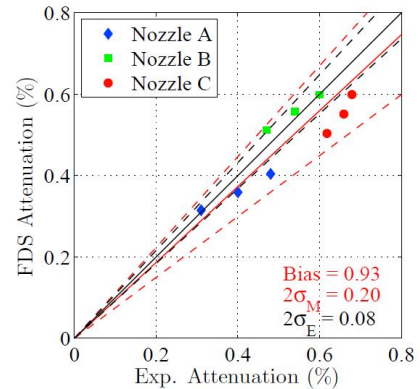
argument should be kept in mind when using the FDS code to simulate the local thermal radiation from a relative small source, such as local pool fire.

A comparison of the simulated and measured attenuations is shown in Figure 7. Average relative experimental uncertainty of $\sigma_E = 0.04$ was assumed. In case of parameter set 1, all the simulations predict less attenuation than what was observed in the experiment. The average bias factor is 0.79 and the relative uncertainty of the simulations is $\sigma_M = 0.21$.

In case of the parameter set 2, the model bias is 0.93 and many of the individual results are within the experimental uncertainty. A clear exception is the Nozzle C, for which the attenuations are still significantly below the experimental values. The explanation can be related to the difference between the ways to prescribe the droplet size distribution between Nozzle C and nozzles A or B. For C, the distribution was based on the number distribution, which resulted in better agreement of the number density in the small range of diameters but increased mean diameter. As the spray absorption and scattering coefficients are based on the Sauter mean diameter d_{32} , the overestimation of the mean diameter is likely to cause underestimated attenuation.



Set 1



Set 2

Figure 7: Comparison of simulated and measured attenuations with parameter sets 1 and 2.

The sensitivity of the attenuation results to the numerical parameters of the model was further investigated by varying the numerical parameters one at the time for nozzle B at 70 bar. The results are summarized Table 4. For most of the parameters, the improved resolution leads to better agreement with the experimental data, consistently with the results shown above. However, the improvement of spatial resolution from 2.0 cm to 1.0 cm decreases the attenuation. The explanation is related to the statistical accuracy of the Lagrangian spray and the ratio of spatial resolution and droplet insertion rate. When the spatial resolution is doubled, the same number of droplets is distributed among 8 times higher number of cells. As a result, some of the cells may have few or zero droplets, and the spray distribution becomes very non-uniform. For the radiation, these regions appear as ‘holes’ in the water shield and the attenuation is decreased.

Table 4: Results of the attenuation sensitivity study for nozzle B at 70 bar pressure.

Parameter	Value	Attenuation	Notes
Experimental result		0.54 ± 0.03	
Spatial resolution (cm)			
	8.0	0.3502	
	4.0	0.4213	
	2.0	0.4734	base case
	1.0	0.3882	
Angular resolution N_{Ω}			
	100	0.3710	
	500	0.4456	
	1000	0.4734	base case
	5000	0.5208	
Droplet insertion rate (1/s)			
	5×10^3	0.1913	$\Delta t_{\text{ins}} = 0.01$ s
	1×10^4	0.3637	
	1×10^5	0.4734	base case
	1×10^6	0.4867	
Droplet CFL-condition			
	∞	0.4734	base case
	1.0	0.4877	
Combined effect			
	$\Delta x = 1.0$ cm		
	NRA = 5000		
	DPS = 1×10^6 1/s	0.5563	
	CFL = 1.0		

CONCLUSIONS

The increasing use of high-pressure water mist systems for fire protection applications has made it necessary to investigate the capabilities of FDS code in the simulation of such systems. This presentation summarizes some of the model enhancements that have been made to improve the accuracy of the high pressure spray simulations in the light of the internal spray properties and the capabilities of the spray to entrain air and attenuate radiation.

The results with one industrial spray nozzle and three fire suppression nozzles showed that the spray properties can be accurately predicted. The simulations were able to predict the V-shaped diameter profile of the LN-2 nozzle, and on the other hand, the flat diameter profiles of the high pressure micro nozzles. The effects of the pressure and multi-orifice spray head characteristics on the air entrainment were correctly predicted. The radiation attenuation results were within the experimental uncertainty when a very good numerical resolution was used, but somewhat under predicted in case of coarser resolution. The conclusion from the radiation sensitivity study was that the spatial resolution should always be in balance with the statistical representation of the spray (number of droplets per second).

The current results form a good basis for the attempts to model complete water mist systems in the conditions of intended applications. We are currently working on publishing the simulation results concerning system activation, cooling performance, flame suppression and effectiveness in the fire protection of complete road tunnels. More work is needed in scaling-up the spray simulations for engineering applications where the spatial resolutions are typically much coarser than what was used here.

ACKNOWLEDGEMENTS

We would like to thank all the members of the FDS development team, and Kevin McGrattan, Randall McDermott and Jason Floyd in particular, for the fruitful co-operation. The work was sponsored by the Finnish Funding Agency for Technology and Innovation, Marioff Corporation Oy, Rautaruukki Oyj, YIT Kiinteistötekniikka Oy and Insinööri-toimisto Markku Kauriala Ltd.

REFERENCES

- Grosshandler, W. L. (2007), A research agenda for the next generation of performance-based design tools. Interflam 2007. International Interflam Conference, 11th Proceedings. Volume 2. September 3-5, 2007, London, England, pp. 1219-1230.

- Hostikka, S., McGrattan, K. (2006), Numerical modeling of radiative heat transfer in water sprays. *Fire Safety Journal* 41, pp. 76-86.
- McGrattan, K.B., Hostikka, S., Floyd, J.E., Baum, H.R., Rehm, R.G., Mell, W.E. and McDermott, R. (2007), *Fire Dynamics Simulator (Version 5), Technical Reference Guide, Volume 1: Mathematical Model*. NIST Special Publication 1018-5, National Institute of Standards and Technology, Gaithersburg, Maryland.
- Prahl, L., Jadoon, A. and Revstedt, J. (2009), Interaction between two spheres placed in tandem arrangement in steady and pulsating flow. *International Journal of Multiphase Flow* 35, pp. 963-969.
- Ramírez-Muñoz, J., Soria, A. and Salinas-Rodríguez, E. (2007), Hydrodynamic force on interactive spherical particles due to the wake effect. *International Journal of Multiphase Flow* 33, pp 802-807.